Heliyon 10 (2024) e36037

Contents lists available at ScienceDirect

Heliyon

journal homepage: www.cell.com/heliyon

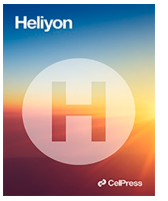

Research article

Musa paradisiaca L. peel extract-bioinspired anisotropic nano-silver with the multipurpose of hydrogenation eco-catalyst and antimicrobial resistance

Hong-Phuong Phan [a,b], Thi-Thanh-Nhi Nguyen [a,b], Thi-Kim-Chi Hua [a,b], Quang-Dong Tu [a,b], Minh-Tam K. Nguyen [a,b], Hoa-Hung Lam [a,b], Thi-Kieu-Anh Tran [a,b], Trung Dang-Bao [a,b,*]

[a] *Faculty of Chemical Engineering, Ho Chi Minh City University of Technology (HCMUT), 268 Ly Thuong Kiet Street, District 10, Ho Chi Minh City, Viet Nam*

[b] *Vietnam National University Ho Chi Minh City, Linh Trung Ward, Thu Duc City, Ho Chi Minh City, Viet Nam*

ARTICLE INFO

Keywords:
Nano-silver
Biosynthesis
Musa paradisiaca L. peel
Eco-catalyst
Kinetics
Thermodynamics
Antimicrobial resistance

ABSTRACT

In an effort to pursue a green synthesis approach, the biosynthesis of nano-silver (nAg) using plant extracts has garnered significant attention, particularly for its antimicrobial resistance and medical applications, which have been the focus of numerous studies. However, there remains a gap in surface catalytic studies, especially regarding the hydrogenation of 4-nitrophenol. While some studies have addressed catalytic kinetics, thermodynamic aspects have been largely overlooked, leaving the catalytic mechanisms of biosynthesized nAg unclear.

In this context, the present work offers a straightforward, eco-friendly, and efficient protocol to obtain nano-silver inspired by *Musa paradisiaca* L. peel extract. This nAg serves multiple purposes, including antimicrobial resistance and as an eco-catalyst for hydrogenation. Predominantly consisting of zero-valent silver with anisotropic polyhedral shapes, mainly decahedra with an edge length of 50 nm, this nAg demonstrated effective antimicrobial action against both *S. aureus* and *E. coli* bacteria.

More importantly, both kinetic and thermodynamic studies on the hydrogenation of 4-nitrophenol to 4-aminophenol catalyzed by this bio-inspired nAg revealed that the rate-limiting step is not diffusion-limited. Instead, the adsorbed hydrogen and 4-nitrophenolate react together via electron transfer on the surface of the nAg. The activation energy of 26.24 kJ mol^{-1} indicates a highly efficient eco-catalyst for such hydrogenation processes.

1. Introduction

Current progress in nanoscience and nanotechnology has provided a robust foundation for diverse fields such as catalysis, antimicrobial applications, sensing, and targeted therapy in medicine [1–7]. Metal nanoparticles, generally defined as being 1−100 nm in size with various shapes, have become fundamental in establishing new synthetic approaches and exploring distinctive

* Corresponding author. Faculty of Chemical Engineering, Ho Chi Minh City University of Technology (HCMUT), 268 Ly Thuong Kiet Street, District 10, Ho Chi Minh City, Viet Nam.
E-mail address: dbtrung@hcmut.edu.vn (T. Dang-Bao).

https://doi.org/10.1016/j.heliyon.2024.e36037
Received 26 February 2024; Received in revised form 6 August 2024; Accepted 8 August 2024
Available online 8 August 2024

physicochemical features. In practice, reports related to top-down synthesis are modest due to surface imperfections of the products and high operating costs [8]. More commonly, metal nanoparticles are obtained via the chemical reduction of metal ions to atoms, followed by their growth to form nuclei and subsequently particles in the nanometer-sized range [9–11]. A stabilizing agent is typically involved during the formation of nanoparticles to prevent agglomeration and ensure better dispersion. Common reducing agents include sodium hydride ($NaBH_4$), hydrazine (N_2H_4), hydrogen gas (H_2), and carbon monoxide (CO) [12]. Generally, the reduction rate when using these strong reducing agents exceeds the growth rate of nuclei, leading to monodispersed metal nanoparticles [13]. However, the use of hazardous substances limits their application in fields related to human health.

Polyphenolics, which are the most representative aromatics with many hydroxyl substituents in plant extracts, are key reagents involved in single electron oxidation, preventing the formation of free radicals in biological systems [14]. Consequently, a significant number of studies have focused on the antioxidant activity of these polyphenolics [15]. Biomolecules present in various plants can serve as reducing agents, facilitating the reduction of metal ions to zero-valent metals. Additionally, the supramolecular structures of polyphenolics can immobilize metal nanoparticles in their networks, preventing aggregation into larger clusters. Thus, plant extracts are widely accepted as safe and efficient constituents for reducing and capping purposes [16–21]. In the pursuit of a green synthesis approach to nanomaterials [22–25], particularly nano-silver/silver nanoparticles [26–34], numerous studies have utilized a wide variety of plant extracts, focusing on their antimicrobial resistance and medical applications. However, the surface catalytic behaviors of natural-origin silver nanoparticles in colloidal solutions have been modestly explored in terms of kinetics and thermodynamics. Generally, catalytic mechanisms have been rarely reported for biosynthesized nano-silver in the literature.

In this study, an aqueous extract of *Musa paradisiaca* L. peel was utilized as a natural-origin reducing and stabilizing agent for the biosynthesis of nano-silver, with the dual purpose of providing antimicrobial resistance (against both gram-positive and gram-negative strains) and serving as an eco-catalyst (for the hydrogenation of 4-nitrophenol in water). Despite numerous reports on the aforementioned applications, the surface activity of silver nanoparticles can be altered by various capping biomolecules [35], leading to differences in antimicrobial and catalytic actions. In particular, the catalytic kinetic and thermodynamic properties were thoroughly studied to explore the corresponding catalytic mechanisms.

2. Experimental

2.1. Synthesis and characterization of Musa paradisiaca L. Peel extract-bio-inspired nano-silver

Unless otherwise stated, all chemical reagents were commercially supplied and directly utilized, including silver nitrate ($AgNO_3$, 99.8 %), sodium borohydride ($NaBH_4$, 99.8 %) from Xilong Scientific, China, and 4-nitrophenol (4-NP, 99 %) from Merck, Germany.

Musa paradisiaca L. peels were washed, dried at 60 °C overnight, and ground into small pieces. The raw material (5.0 g) was immersed in 100.0 mL deionized water, then magnetically stirred at 500 rpm and 80 °C for 10 min. After centrifugation and vacuum filtration using filter paper, the aqueous extract solution was stored in a dark bottle at 4 °C for further use. Total phenolic content was determined by the Folin-Ciocalteu method. The reaction mixture, composed of the extract (1.0 mL, a 10-fold dilution), 10 % Folin−Ciocalteu reagent (5.0 mL) and 7.5 % sodium carbonate (4.0 mL), was allowed to stand at room temperature for 45 min. The absorbance of the reaction mixture was measured at a wavelength of 765 nm. Total phenolic content in the extract solution (mg/L) was reported as gallic acid equivalents (GAE), and the results were presented as average values for triplicates.

Nano-silver nanoparticles (nAg) were synthesized via the chemical reduction of $AgNO_3$, bioinspired by polyphenols derived from the *Musa paradisiaca* L. peel extract, which acted as reducing and stabilizing agents. Typically, the extract solution (10.0 mL) was added to the $AgNO_3$ aqueous solution, yielding a final volume of 60.0 mL and a constant silver concentration of 1.0 mM. The reaction mixture was magnetically stirred at 300 rpm and 70 °C for 120 min. The effects of synthetic conditions on the formation of nAg were studied, including duration (0−150 min), temperature (50−80 °C), and volume of the extract (5.0−20.0 mL). A single-factor optimization was performed by changing one factor while keeping the others constant as in the typical procedure. The resulting solutions were 3-fold diluted using deionized water before measuring their absorbance on an Optizen Pop UV–Vis spectrophotometer (KLab, Republic of Korea), using a 1-cm path length quartz cuvette. The size and shape of nAg were inspected using a JEOL JEM 2100F transmission electron microscope (TEM). Solid-state nAg was obtained by centrifuging at 10,000 rpm. Fourier-transform infrared spectroscopy (FT-IR) was performed on a Tensor 27 Bruker instrument using KBr pellets for sample preparation. X-ray diffraction (XRD) analysis was conducted on a D2 Phaser Bruker instrument using Cu-Kα radiation ($\lambda = 1.5406$ Å) at 40 kV and 30 mA.

2.2. Antimicrobial resistance of bio-inspired nano-silver

The antimicrobial activity against gram-positive (+) *Staphylococcus aureus* ATCC 29213 (*S. aureus*) and gram-negative (−) *Escherichia coli* ATCC 25922 (*E. coli*) was examined via the zone of inhibition (ZOI) method and the minimum inhibitory concentration (MIC) method.

The bacterial strains were precultured at 37 °C for 24 h in Mueller Hinton Broth (MHB) medium. After being diluted in MHB, vortexed evenly, and adjusted to a bacterial suspension concentration of 10^8 CFU/mL, bacterial solutions (200 μL) were spread onto Mueller Hinton Agar (MHA) medium. After drying, holes were punched into the agar, and 50 μL of the nAg solution was added to each hole. The agar plates were then incubated at 37 °C for 24 h. The ZOI diameter was determined as the median value of three replicates, compared with the control using 50 μL of the extract solution.

The MIC was defined as the lowest concentration inhibiting bacterial growth after 24 h of preculture, determined by a resazurin-based 96-well plate microdilution method. Each well consisted of 50 μL of bacterial solution at a concentration of 10^6 CFU/mL, nAg

solution diluted with the medium (N/2, N/4, N/8, N/16, N/32, N/64, where N = 1.0 mM), and MHB added to make up 100 μL. Two control samples were used: (i) MHB medium with a bacterial strain as a positive control, and (ii) only MHB medium as a negative control. The wells were aerobically incubated at 37 °C for 24 h. After incubation, 50 μL of 0.15 % resazurin was added to the wells and incubated for 2 h, recording the color change in comparison with the color of resazurin. The MIC assays were conducted in triplicate for each type of bacteria.

2.3. Catalytic reactivity of bio-inspired nano-silver in the hydrogenation of 4-nitrophenol

As a benchmark experiment, the selective hydrogenation of 4-nitrophenol (4-NP) to 4-aminophenol (4-AP) in water was performed in a 1-cm quartz cuvette at room temperature using the following optimized parameters: 0.1 mL of 2.5 mM 4-NP aqueous solution and 0.1 mL of $NaBH_4$ aqueous solution (a molar ratio of $NaBH_4$/4-NP of 200/1) were added to 1.0 mL of the as-prepared nAg aqueous solution. Distilled water was then added to make a total volume of 2.5 mL for the reaction solution. During the 10-min reaction period, the absorbance of the reaction solution was monitored using an Optizen Pop UV–Vis spectrophotometer (KLab, South Korea) at wavelengths ranging from 200 to 600 nm.

3. Results and discussion

3.1. Physicochemical features of bio-inspired nano-silver

As one of the most universal food crops originating from tropical countries, the economic exploitation of *Musa paradisiaca* L. peel has been largely restricted to its use as a source of antioxidants in food additives [36]. The major polyphenolics discovered in *Musa paradisiaca* L. peel include phenolic acids, flavonoids, and anthocyanins, which can act as both reducing and stabilizing agents for the formation of metal nanoparticles. To the best of our knowledge, the utilization of an aqueous extract of *Musa paradisiaca* L. peel in the bio-inspired synthesis of nano-silver (nAg) for multifunctional purposes in catalysis and antimicrobial applications has not been reported, despite the popularity of similar strategies.

In principle, the chemical reduction ability of Ag(I) ions to zero-valent silver Ag(0) is widely recognized and is associated with the antioxidant activities of plant extracts, mainly due to the oxidation of hydroxyl groups to aldehydes or carboxylic acids [19–21]. Furthermore, these biomolecules in plant extracts can serve as stabilizing agents through steric or electrostatic effects, preventing the agglomeration of small nanoparticles into larger clusters.

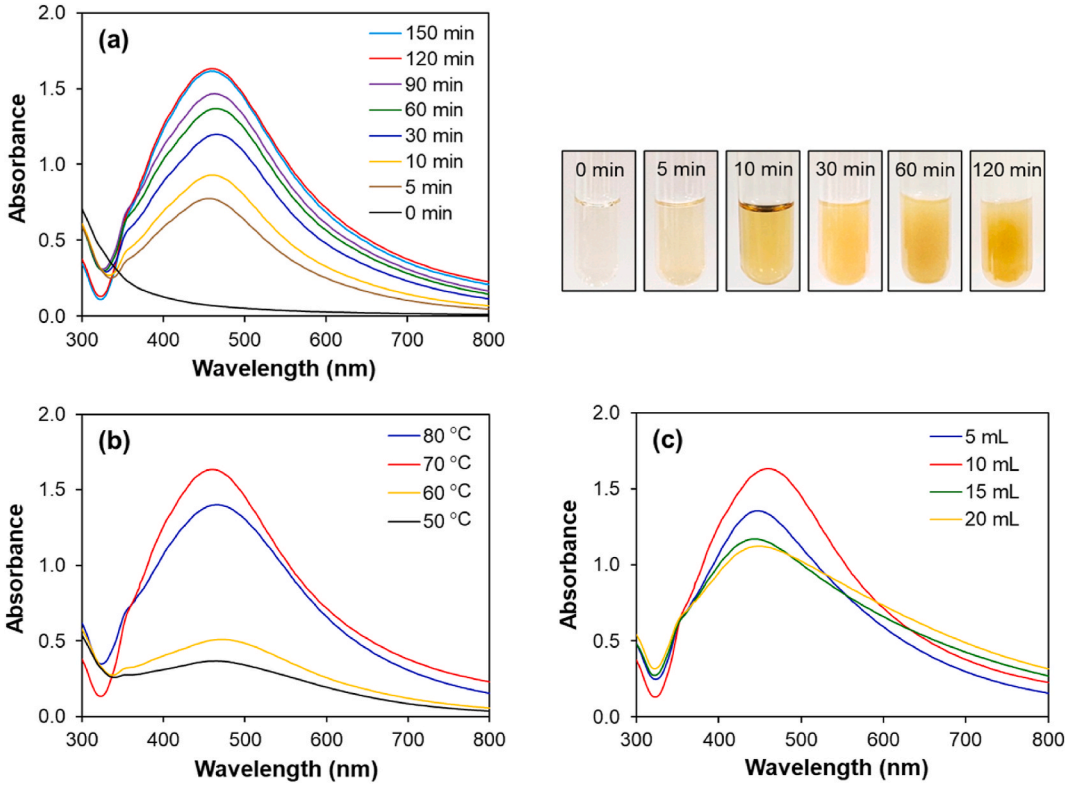

Fig. 1. UV–vis spectra of nAg solutions governed by various conditions (a) duration (with their photos inset), (b) temperature, and (c) volume of the extract.

Aiming to potentially access antibacterial and medical applications, the use of any external chemicals in the synthesis was strictly avoided, except for a silver precursor ($AgNO_3$) and an aqueous solution of the plant extract. At 70 °C, the gradual formation of nAg in a colloidal solution over time was monitored using UV–Vis spectroscopy (Fig. 1a). After only 5 min, an absorption band centered at a wavelength of 460 nm was observed, corresponding to the surface plasmon resonance (SPR) of nAg [37]. Over time, the SPR band of nAg significantly increased in intensity during the first 60 min and reached its maximum after 120 min. Higher SPR intensity indicates a greater quantity of particles [13]. This suggests that the chemical reduction of Ag(I) ions to Ag(0) was completed within 120 min and the concentration of nAg reached saturation following nucleation and particle growth. During the 120-min duration, the reaction solution changed from colorless (attributed to Ag(I) ions) to pale yellow and finally dark yellow, corresponding to an increase in particle concentration. Extending the reaction time to 150 min resulted in a slight decrease in absorption intensity, indicating the beginning of nAg coalescence into larger particles. Therefore, the synthesis should be stopped at 120 min.

The effect of temperature on the formation of nAg in an aqueous solution was also investigated (Fig. 1b). The reaction rate is known to be temperature-dependent; hence, increasing the temperature from 50 °C to 70 °C accelerated the reduction rate of Ag(I) ions, producing a higher number of nAg. Consequently, the SPR absorption band reached its peak at 70 °C. A faster reaction rate resulted from more frequent collisions, affecting not only the reduction but also nucleation and particle coalescence. This explains why the SPR absorption band of nAg decreased at 80 °C, suggesting that oversaturation led to nAg aggregation.

The volume of the extract, which influences its reducing ability, was also an important factor determining the reduction rate. Using 10 mL of the extract yielded the highest SPR absorption intensity (Fig. 1c) compared to smaller volumes (5 mL) or larger volumes (15 mL or 20 mL) of the extract. A small volume (5 mL) contained insufficient reducing biomolecules for effective chemical reduction. Conversely, lower and broader absorption bands were observed with larger volumes (15 mL and 20 mL), likely due to a surface capping

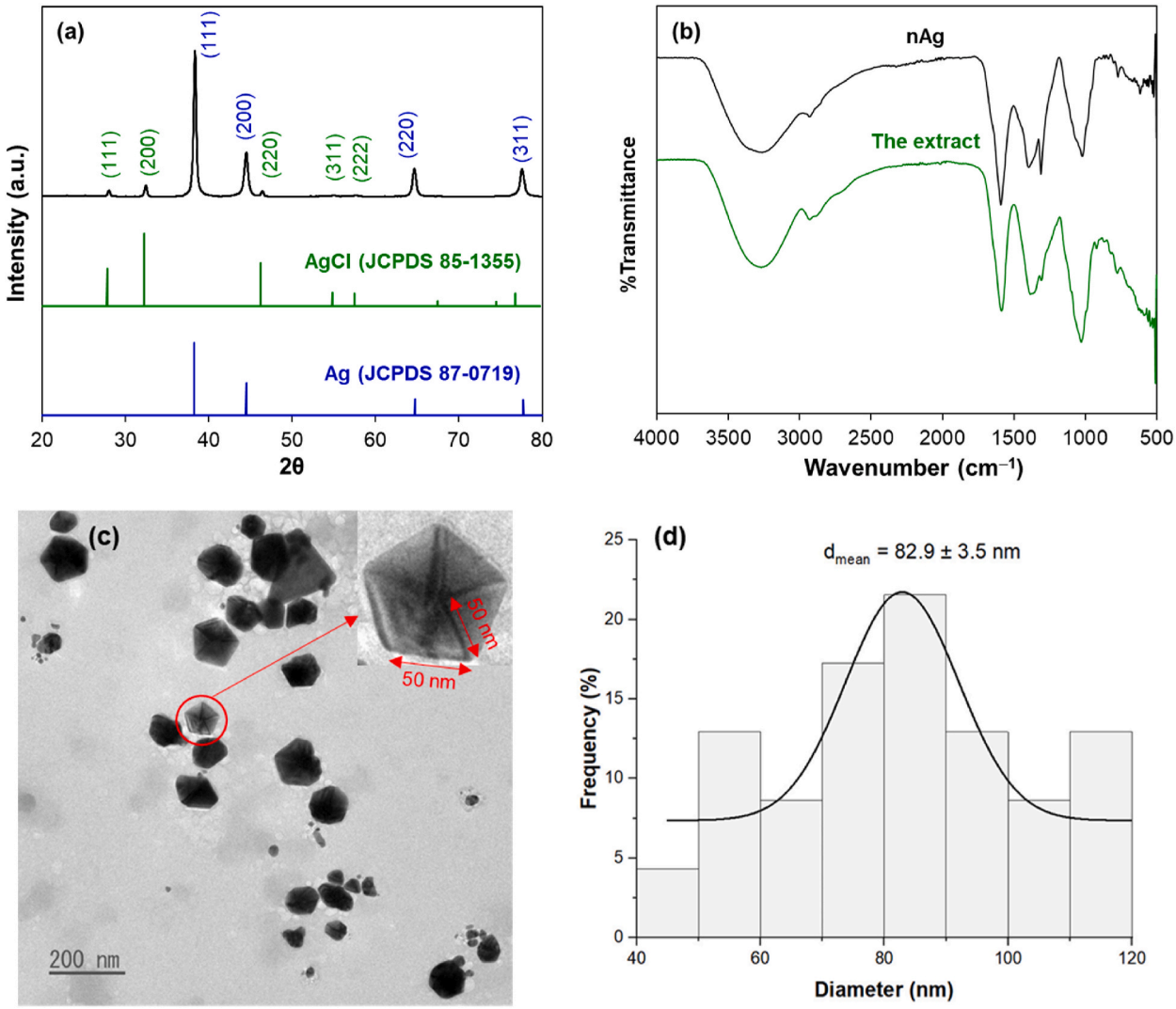

Fig. 2. (a) XRD pattern, (b) FT-IR spectra, (c) TEM image, and (d) size distribution histogram of nAg.

effect [13]. A thick layer of stabilizing biomolecules on the surface of the nAg significantly interfered with the SPR effect. Additionally, the color of the reaction solution became darker with increased extract volume, affecting absorbance measurement. Thus, 10 mL of the extract was chosen for the synthesis procedure.

In summary, the optimized nAg synthesis procedure was established as follows: 60 mL of an aqueous solution consisting of 1.0 mM $AgNO_3$ and 10 mL of the extract was reacted at 70 °C for 120 min.

The presence of nAg in the solid state was explored using XRD (Fig. 2a). The diffraction peaks centered at 2θ of 38.3°, 44.5°, 64.7°, and 77.7° represented the crystal planes of (111), (200), (220), and (311), respectively [38]. According to the XRD standard JCPDS 87–0719, these results confirmed the formation of a face-centered cubic (fcc) crystalline structure of zero-valent silver. Using the Scherrer equation, the crystallite size at the (111) plane was estimated to be 21.7 nm. Although no silver oxides or hydroxides were detected, it was interesting that the face-centered cubic (fcc) crystalline phase of AgCl was also identified (JCPDS 85–1355). A nanocomposite of Ag/AgCl was obtained instead of pure silver nanoparticles, likely due to a precipitation reaction between Ag(I) and Cl(I) ions from the extract's phytochemical constituents [39–41]. Furthermore, the signal intensity of Ag(0) was much higher than that of AgCl, indicating that silver nanoparticles were the major component. This result contrasts with previous reports; for instance, Khan et al. did not detect AgCl in *Medicago polymorpha*-mediated silver nanoparticles [40], while Rattanakit et al. observed a much higher intensity of the AgCl signal than Ag(0) using *Clitoria ternatea* flower [41]. These differences could be attributed to the diverse phytochemical constituents in various plants, resulting in variations in the obtained nAg and their reactivity in catalysis and antibacterial applications.

The chemical constituents of the obtained nAg and the extract were explored via vibrational bands in FT-IR spectra (Fig. 2b). Generally, the two spectra showed similarities in absorption bands, as phytochemical constituents (polyphenolics) were primarily detected in both samples. Typically, the absorption bands centered at 3268 cm^{-1}, 2900 cm^{-1}, 1600 cm^{-1}, and 1028 cm^{-1} represented the stretching vibrations of O–H (hydroxyl from phenolics), C–H (methylene), C=O (aldehyde, carboxylic acid, ester, carbonyl), and C–O–C, respectively [40,41]. Compared to the extract sample, the bending vibration of O–H groups centered at 1383 cm^{-1} and the stretching vibration of O–H groups centered at 3268 cm^{-1} were lower in intensity in the nAg sample, likely due to a decrease in the number of O–H groups. The chemical reduction of Ag(I) to Ag(0) occurred alongside the oxidation of hydroxyl groups to aldehyde or carboxylic groups, resulting in increased intensity of the C=O absorption band. Additionally, the appearance of more C–H vibrational bands from aldehydes likely influenced the shape of the peak at 2900 cm^{-1}, making it sharper. This result was consistent with the determination of total phenolic content for the extract (468 mg/L) and the nAg solution (82 mg/L), showing a significant decrease in the number of hydroxyl groups of phytochemical constituents during nAg synthesis. Furthermore, the strong affinity of hydroxyl and carboxyl groups towards the surface of nAg resulted in its stabilization, preventing aggregation into larger clusters. Thus, biomolecules acted as both reducing agents and stabilizers [40,41].

The presence of nAg in a colloidal solution was observed via TEM image (Fig. 2c), which showed their size-based monodispersity (Fig. 2d). Their morphologies were anisotropic polyhedrons, primarily decahedra with an edge length of approximately 50 nm.

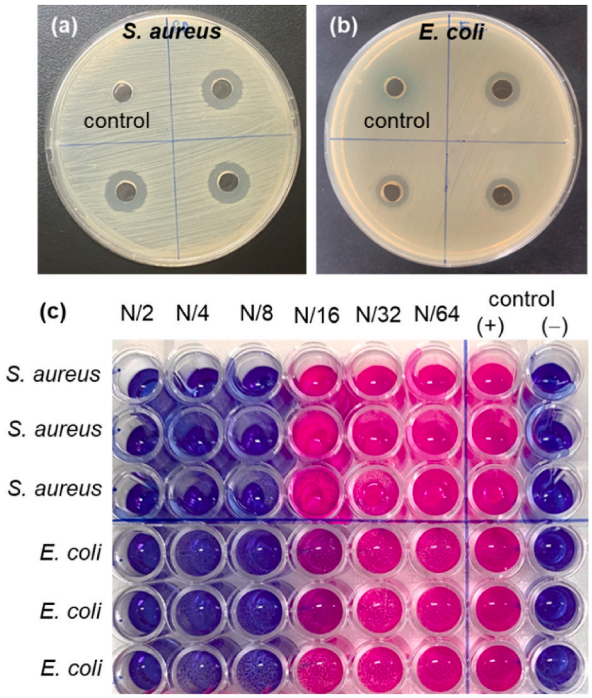

Fig. 3. Antimicrobial activity of nAg against *S. aureus*, and *E. coli* bacteria using (a, b) a ZOI method, and (c) a MIC method.

3.2. Antimicrobial resistance of bio-inspired nano-silver

Over the past decade, there have been a record number of reports on the antibacterial resistance of silver nanoparticles against diverse gram-positive and gram-negative bacteria. There have been ongoing efforts to establish a unified mechanism for their antibacterial efficacy. Generally, most previous studies have highlighted the influences of size, shape, and composition of silver nanoparticles on their antibacterial performances via various mechanisms [42–44]. The most widely accepted mechanism involves silver ions generated from nanoparticles interfering with the replication of DNA, preventing the division of microbial cells and thus killing them. Silver ions also interact with nucleic acids, leading to their destruction. Additionally, silver ions can induce the formation of oxygen free radicals, which are toxic to microbial cells. According to the Ostwald–Freundlich equation, silver nanoparticles with small sizes and spherical shapes facilitate the release of silver ions [45]. Therefore, most previous works reported high antibacterial activity of biosynthesized nAg with a spherical shape. Another mechanism involves nAg breaking the cell membrane of bacteria, resulting in a strong interaction between nAg and sulfur/phosphorus groups present in cellular components. Consequently, the structures and functions of DNA and proteins can be modified. In this manner, nAg in a truncated triangular shape showed good antimicrobial action as their edges efficiently cut through the cell membranes [44].

In this work, the antimicrobial activity of as-prepared nAg against gram-positive (+) *Staphylococcus aureus* (*S. aureus*) and gram-negative (−) *Escherichia coli* (*E. coli*) was examined using a zone of inhibition (ZOI) method and a minimum inhibitory concentration (MIC) method (Fig. 3). The ZOI diameters of as-prepared nAg were measured to be 14.1 ± 0.1 mm for *S. aureus* and 11.4 ± 0.1 mm for *E. coli*. No zone of inhibition was observed for the control samples, indicating that the antimicrobial activity against both types of bacteria was primarily due to nAg (Fig. 3a and b). The antimicrobial activity against both *S. aureus* and *E. coli* was clearly observed in the presence of nAg, as indicated by the blue color. When the concentration of nAg decreased, the pink color was observed, evidencing their inactivation against bacteria. In this case, nAg showed complete inhibition against both types of bacteria at a MIC value of N/8, which is 13.5 μg/mL (Fig. 3c). The results of the antimicrobial activity of as-prepared nAg against *S. aureus* and *E. coli* are summarized in Table 1. In general, the antibacterial efficacy against the gram-positive strain was better than that against the gram-negative strain. This could be due to differences in their cell wall structure and metabolism, as well as their interaction with nAg capped by different biomolecules [46]. It was also noted that the presence of AgCl could enhance its antimicrobial action, with chlorine free radicals acting as strong oxidative agents, reacting with cellular biocomponents [47].

3.3. Catalytic reactivity of bio-inspired nano-silver in the hydrogenation of 4-nitrophenol

To evaluate the catalytic characteristics of nanostructured materials, the selective hydrogenation of 4-nitrophenol (4-NP) to 4-aminophenol (4-AP) using $NaBH_4$ as a reducing agent has emerged as a model catalytic reaction. The popularity of this reaction can be attributed to the following factors: (i) its simplicity; (ii) the 4-nitrophenolate ions absorb visible light, allowing for easy monitoring by spectrophotometric methods; (iii) the reaction does not proceed in the absence of a catalyst, and no side reactions are observed [48,49]. According to the widely accepted Langmuir-Hinshelwood mechanism, the 4-nitrophenolate ions (which mainly exist in an alkaline environment) and the hydrogen species (generated from BH_4^- ions) are adsorbed on the surface of nAg, where electron transfer occurs. Subsequently, 4-aminophenol is produced as the exclusive product [38,48–52].

In this work, the catalytic reactivity of bio-synthesized nAg was investigated in the selective hydrogenation of 4-NP to 4-AP in water using $NaBH_4$ as a hydrogen source. At room temperature, the reaction was monitored by UV–vis spectrophotometry (Fig. 4a), with maximum absorption bands centered at 400 nm (attributed to 4-NP in the form of 4-nitrophenolate) and 300 nm (attributed to 4-AP) [38,52]. As the reaction progressed, a decrease in absorption intensity at 400 nm and an increase in absorption intensity at 300 nm indicated the conversion of 4-NP to 4-AP. Furthermore, the appearance of two isosbestic points at 275 nm and 320 nm confirmed the exclusive production of 4-AP, eliminating the possibility of side reactions [38,52]. Under benchmark conditions, the catalytic hydrogenation of 4-NP achieved a 91 % conversion after 10 min, and the reaction solution turned from yellow to colorless.

The effect of the molar ratio of $NaBH_4$/4-NP on the reaction rate was also examined, as shown in Fig. 4b. In the absence of $NaBH_4$ (a ratio of 0/1), no reaction occurred after 6 min, indicating that surface hydrogen generated from $NaBH_4$ was essential for the hydrogenation. Increasing the amount of $NaBH_4$ (with ratios from 100/1 to 200/1) accelerated the reaction, as evidenced by a dramatic decrease in absorption intensity at 400 nm. However, using an excess of $NaBH_4$ (such as a ratio of 250/1) resulted in negligible additional increase in reaction rate, likely due to the formation of excess surface hydrogen species interfering with the approach of 4-nitrophenolate to the catalytic sites [49]. Therefore, the optimal molar ratio of $NaBH_4$/4-NP for the reaction was determined to be 200/1.

A blank test conducted under benchmark conditions without nAg confirmed the catalytic role of bio-synthesized nAg, as no reaction occurred. Increasing the concentration of the silver catalyst further accelerated the reaction, as indicated by an increase in the reaction rate constant (Fig. 4c). Given the significantly larger mole ratio of $NaBH_4$ to 4-NP, this catalytic hydrogenation was expected to follow a

Table 1
Antimicrobial activity of nAg against *S. aureus*, and *E. coli* bacteria.

Bacteria	ZOI diameter[a] (mm)	MIC (μg/mL)
S. aureus	14.1 ± 0.1	13.5 (N/8)
E. coli	11.4 ± 0.1	13.5 (N/8)

[a] Mean value ± standard deviation of three replicates.

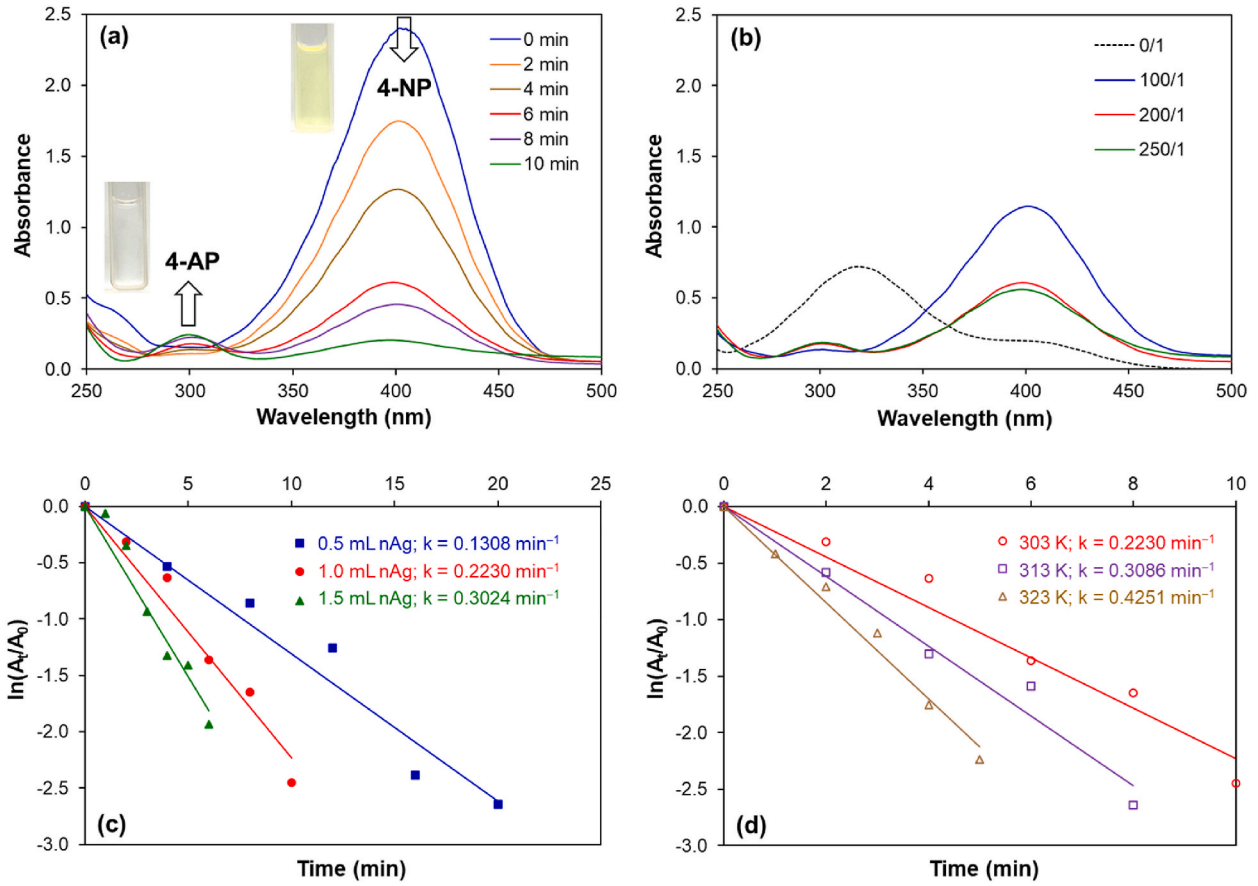

Fig. 4. Investigation on catalytic reactivity of nAg in the hydrogenation of 4-NP by varying operating conditions: (a) reaction time, (b) $NaBH_4$/4-NP molar ratio, (c) silver catalyst concentration at room temperature, and (d) reaction temperature.

pseudo-first-order kinetic model rather than a second-order model, as described by the following equation [38,48–52].

$$\ln\frac{C_t}{C_0} = \ln\frac{A_t}{A_0} = -kt$$

Where C_0 and C_t, A_0 and A_t represent the concentrations of 4-NP and the corresponding absorbances recorded at 400 nm at the initial and at any given time, respectively; t represents the reaction duration; and k represents the apparent kinetic rate constant.

The plot of (A_t/A_0) versus reaction time produced straight lines with negative slopes and high determination coefficients ($R^2 > 98$ %), allowing for the determination of reaction rate constants at various catalyst concentrations (Fig. 4c). A higher reaction rate

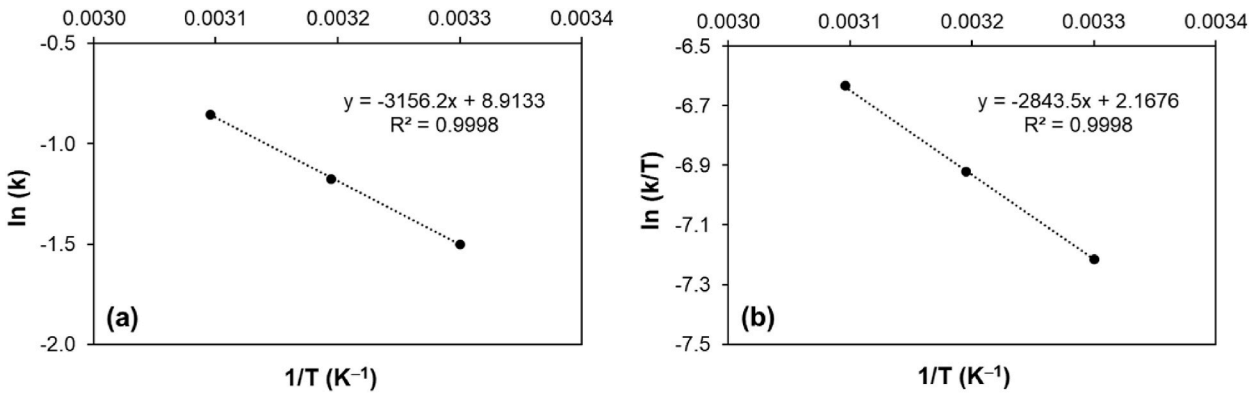

Fig. 5. (a) The Arrhenius plot ln(k), and (b) the Eyring plot ln(k/T) versus 1/T for the hydrogenation of 4-NP catalyzed by nAg.

constant indicates a faster reaction rate [53].

Within the temperature range of 303–323 K, the reaction rate for the catalytic hydrogenation of 4-NP increased with rising temperature, consistent with collision theory (Fig. 4d) [54,55]. A strong linear relationship between ln(k) versus 1/T enabled the determination of the activation energy (E_a) (Fig. 5a). Similarly, plotting ln(k/T) versus 1/T provided values for the activation enthalpy ($\Delta H^{\#}$) and activation entropy ($\Delta S^{\#}$), with excellent determination coefficients ($R^2 = 0.9998$) (Fig. 5b) [55,56]. These thermodynamic parameters for the hydrogenation of 4-NP catalyzed by nAg are summarized in Table 2.

The activation energy reflects the nature of the metal nano-catalysts; generally, a lower activation energy indicates a more efficient catalyst and an easier catalytic process. For this study, the activation energy for the hydrogenation of 4-NP catalyzed by nAg was estimated to be 26.24 kJ mol^{-1}, which is lower compared to values reported for other metal nano-catalysts [55–61]. This suggests that the rate-limiting step involves the reaction between adsorbed hydrogen and 4-nitrophenolate via electron transfer on the nAg surface, as opposed to a diffusion-limited mechanism, which typically has an activation energy below 20 kJ mol^{-1} [54]. This result supports the Langmuir-Hinshelwood mechanism.

The activation enthalpy for the hydrogenation of 4-NP was found to be 23.64 kJ mol^{-1}, and the activation entropy was −213.55 J mol^{-1} K^{-1}. The positive value of $\Delta H^{\#}$ indicates that the catalytic process is endothermic, aligning with the observed increase in reaction rate constant with rising temperature (Fig. 4d). The negative $\Delta S^{\#}$ reflects a decrease in activation entropy, suggesting that the transition states involve more ordered structures. This is consistent with the first-order kinetics, where 4-nitrophenolate and BH_4^- ions adsorb onto the nAg surface to form a well-defined activated complex [55]. In summary, this work demonstrates an efficient and effective nano-catalyst for the hydrogenation of 4-NP to 4-AP in water.

A comparative survey of the catalytic activity of natural-origin silver nanoparticles in the hydrogenation of 4-NP to 4-AP using $NaBH_4$ at room temperature is summarized in Table 3. In this study, the silver nanoparticles were obtained in anisotropic polyhedral shapes, primarily decahedra, differing from the spherical shapes reported in the literature [61–65]. Despite the larger size of the present nAg, its catalytic activity appears superior. This enhanced activity can be attributed to the shape of the nanoparticles. In surface-catalytic processes, the surface structure of metal nanoparticles significantly influences their catalytic performance. While the impact of size on catalytic activity has been extensively documented, shape dependence has been less studied [66]. In the catalytic mechanism described, the rate-limiting step involves the reaction between adsorbed hydrogen and 4-nitrophenolate through electron transfer on the nAg surface. Therefore, the high electron density at the sharp edges and corners of the decahedral shape enhances the reaction rate [66].

Previous studies have predominantly focused on the kinetic aspects of catalysis, whereas this work provides insights into the catalytic mechanism through thermodynamic analysis.

4. Conclusions

This study presents a straightforward, eco-friendly, and efficient method for producing *Musa paradisiaca* L. peel extract-bioinspired nano-silver (nAg). The reduction of Ag(I) ions to zero-valent Ag(0) was facilitated by the antioxidant activities of the plant extract, which are primarily linked to the oxidation of hydroxyl groups to aldehydes or carboxylic acids. Additionally, these biomolecules acted as stabilizing agents through steric and electrostatic effects, preventing the agglomeration of nAg. Besides the predominant zero-valent silver, the presence of AgCl in the nanocomposite resulted from the precipitation reaction between Ag(I) and Cl(I) ions, which originated from the phytochemical constituents of the extract. The nAg exhibited anisotropic polyhedral shapes, primarily decahedra, with edge lengths around 50 nm.

The results demonstrate the multifunctional properties of the bio-inspired nAg as both an antimicrobial agent and an eco-catalyst for hydrogenation. Its effective antimicrobial action against both *S. aureus* and *E. coli* can be attributed to the efficient disruption of cell membranes by the nAg edges and the reaction of chlorine free radicals from AgCl with cellular components. Regarding its catalytic performance, the hydrogenation of 4-nitrophenol to 4-aminophenol followed a pseudo first-order kinetic model, with an apparent rate constant of 0.2230 min^{-1} at room temperature. The thermodynamic analysis revealed an activation enthalpy of 23.64 kJ mol^{-1}, an activation entropy of −213.55 J mol^{-1} K^{-1}, and an activation energy of 26.24 kJ mol^{-1}, indicating that the rate-limiting step involves the reaction between adsorbed hydrogen and 4-nitrophenolate via electron transfer on the nAg surface, rather than a diffusion-limited mechanism. In summary, this study provides an efficient eco-catalyst and elucidates its catalytic mechanism for the hydrogenation reaction.

Table 2
Thermodynamic parameters for the hydrogenation of 4-NP catalyzed by nAg.

Thermodynamic studies		Parameters		R^2
Arrhenius	$\ln(k) = \ln(A) - \frac{E_a}{RT}$	E_a (kJ mol^{-1})	26.24	0.9998
Eyring	$\ln\left(\frac{k}{T}\right) = \ln\left(\frac{k_B}{h}\right) + \frac{\Delta S^{\#}}{R} - \frac{\Delta H^{\#}}{RT}$	$\Delta H^{\#}$ (kJ mol^{-1}) $\Delta S^{\#}$ (J mol^{-1} K^{-1})	23.64 −213.55	0.9998

Where: k = apparent kinetic rate constant, A = Arrhenius factor, E_a = activation energy, R = the ideal gas constant, T = absolute temperature, k_B = the Boltzmann constant, h = the Planck constant, $\Delta H^{\#}$ = activation enthalpy, $\Delta S^{\#}$ = activation entropy, and R^2 = determination coefficient.

Table 3
Comparison of catalytic activity of bio-inspired nAg in the hydrogenation of 4-NP towards 4-AP by $NaBH_4$ at room temperature.

Plant source	Shape, size	4-NP (mM)	$NaBH_4$/4-NP	Catalytic efficiency	E_a (kJ mol^{-1})	Ref.
Musa paradisiaca L. peel	Anisotropic polyhedrons (decahedra, 50 nm edge length)	0.10	200/1	91 %, 10 min	26.24	This work
Tulsi leaf	Sphere, 5−10 nm	0.09	400/1	100 %, 30 min	40.25	[61]
Polar seaweed *Fucus gardeneri*	Sphere, 19 nm	0.21	50/1	96 %, 5 min	n.r.	[62]
Trachyspermum ammi (*Ajwain*) seed	Sphere, 5−20 nm	0.05	300/1	100 %, 12 min	n.r.	[63]
Breynia rhamnoides stem	Sphere, 64 nm	0.2	50/1	70 %, 15 min	n.r.	[64]
Acacia nilotica stem	Sphere, <50 nm	0.08	200/1	94 %, 10 min	n.r.	[65]

n. r. = not reported.

Data availability

Data included in article.

CRediT authorship contribution statement

Hong-Phuong Phan: Writing – original draft, Validation, Methodology, Formal analysis, Data curation, Conceptualization. **Thi-Thanh-Nhi Nguyen:** Investigation, Formal analysis. **Thi-Kim-Chi Hua:** Investigation, Formal analysis. **Quang-Dong Tu:** Investigation, Formal analysis. **Minh-Tam K. Nguyen:** Methodology, Formal analysis, Data curation. **Hoa-Hung Lam:** Methodology, Formal analysis, Data curation. **Thi-Kieu-Anh Tran:** Methodology, Formal analysis. **Trung Dang-Bao:** Writing – review & editing, Writing – original draft, Visualization, Validation, Supervision, Methodology, Formal analysis, Conceptualization.

Declaration of competing interest

The authors declare that they have no known competing financial interests or personal relationships that could have appeared to influence the work reported in this paper.

Acknowledgements

We acknowledge Ho Chi Minh City University of Technology (HCMUT), VNU-HCM for supporting this study.

References

[1] R.V. Bordiwala, Results in Chemistry 5 (2023) 100832.
[2] M.Q. He, Y. Ai, W. Hu, L. Guan, M. Ding, Q. Liang, Adv. Mater. 35 (2023) 2211915.
[3] P.G. Jamkhande, N.W. Ghule, A.H. Bamer, M.G. Kalaskar, J. Drug Deliv. Sci. Technol. 53 (2019) 101174.
[4] T.H. Le-Lam, H.H. Lam, H.P. Phan, T. Nguyen, T. Dang-Bao, Mater. Today: Proc. 66 (2022) 2720–2725.
[5] A. Reina, T. Dang-Bao, I. Guerrero-Ríos, M. Gómez, Nanomaterials 11 (2021) 1891.
[6] J. Yuan, Y. Wang, W. Yang, X. Li, K. Tao, W. He, J. Yan, Chem. Eng. J. 470 (2023) 144266.
[7] Z. Jiang, X. Han, C. Zhao, S. Wang, X. Tang, Int. J. Mol. Sci. 23 (2022) 1923.
[8] T. Dang-Bao, I. Favier, M. Gómez, Metal nanoparticles in polyols: bottom-up and top-down syntheses and catalytic applications, in: K. Philippot, A. Roucoux (Eds.), Nanoparticles in Catalysis: Advances in Synthesis and Applications, Wiley-VCH GmbH, Weinheim, Germany, 2021, pp. 99–122.
[9] T.K.T. Nguyen, N. Maclean, S. Mahiddine, Chem. Rev. 114 (2014) 7610–7630.
[10] J. Polte, CrystEngComm 17 (2015) 6809–6830.
[11] K.J. Wu, C.M. Edmund, C. Shang, Z. Guo, Prog. Mater. Sci. 123 (2022) 100821.
[12] K. Philippot, A. Roucoux, Nanoparticles in Catalysis: Advances in Synthesis and Applications, Wiley-VCH GmbH, Weinheim, Germany, 2021.
[13] T. Dang-Bao, N.H. Le, H.H. Lam, Chemical Engineering Transactions 97 (2022) 331–336.
[14] J.G. Handique, J.B. Baruah, React. Funct. Polym. 52 (2002) 163–188.
[15] Y. Lang, N. Gao, Z. Zang, X. Meng, Y. Lin, S. Yang, Y. Yang, Z. Jin, B. Li, Journal of Future Foods 4 (2024) 193–204.
[16] S.U.R. Qamar, J.N. Ahmad, J. Mol. Liq. 334 (2021) 116040.
[17] G. Karunakaran, K.G. Sudha, S. Ali, E.B. Cho, Molecules 28 (2023) 4527.
[18] K.K. Brar, S. Magdouli, A. Othmani, J. Ghanei, V. Narisetty, R. Sindhu, P. Binod, A. Pugazhendhi, M.K. Awasthi, A. Pandey, Environ. Res. 207 (2022) 112202.
[19] F. Moradi, S. Sedaghat, O. Moradi, S.A. Salmanabadi, Inorganic and Nano-Metal Chemistry 51 (2021) 133–142.
[20] N. Rani, P. Singh, S. Kumar, P. Kumar, V. Bhankar, K. Kumar, Mater. Res. Bull. 163 (2023) 112233.
[21] A.R. Bagheri, N. Aramesh, M.S. Hasnain, A.K. Nayak, R.S. Varma, Chemical Physics Impact 7 (2023) 100255.
[22] M. Abbasi, S.R. Kasaee, H. Kamyab, S. Chelliapan, I. Kirpichnikova, Z.H. Mussa, A.M. Amani, S. Mosleh-Shirazi, Appl. Phys. A 130 (2024) 284.
[23] L. Shabani, S.R. Kasaee, S. Chelliapan, M. Abbasi, H. Khajehzadeh, F.S. Dehghani, T. Firuzyar, M. Shafiee, A.M. Amani, S. Mosleh-Shirazi, A. Vaez, H. Kamyab, Appl. Phys. A 129 (2023) 564.
[24] A. Nasibova, Advances in Biology & Earth Sciences 8 (2023) 140–146.

[25] C. Keskin, A. Baran, M.F. Baran, A. Hatipoğlu, M.T. Adican, M.N. Atalar, I. Huseynova, R. Khalilov, E. Ahmadian, Ö. Yavuz, S.İ. Kandemir, A. Eftekhari, J. Nanomater. 2022 (2022) 7211066.
[26] J. Xu, M. Yıldıztekin, D. Han, C. Keskin, A. Baran, M.F. Baran, A. Eftekhari, C.A. Ava, S.İ. Kandemir, D.B. Cebe, B. Dağ, A. Beilerli, R. Khalilov, Heliyon 9 (2023) e19061.
[27] A.F. Jafarova, V.N. Ramazanli, Advances in Biology & Earth Sciences, vol. 5, 2020, pp. 218–223.
[28] A. Baran, M.F. Baran, C. Keskin, S.I. Kandemir, M. Valiyeva, S. Mehraliyeva, R. Khalilov, A. Eftekhari, J. Nanomater. 2021 (2021) 2270472.
[29] F. Gheisari, S.R. Kasaee, P. Mohamadian, S. Chelliapan, R. Gholizadeh, Z. Zareshahrabadi, S.P. Solhjoo, E. Vafa, S. Mosleh-Shirazi, A.M. Amani, H. Kamyab, Inorg. Chem. Commun. 161 (2024) 112006.
[30] S. Mosleh-Shirazi, M.A.J. Kouhbanani, N. Beheshtkhoo, S.R. Kasaee, A. Jangjou, P. Izadpanah, A.M. Amani, Appl. Phys. A 127 (2021) 857.
[31] M. Abbasi, R. Gholizadeh, S.R. Kasaee, A. Vaez, S. Chelliapan, F.F. Al-Qaim, I.F. Deyab, M. Shafiee, Z. Zareshahrabadi, A.M. Amani, S. Mosleh-Shirazi, H. Kamyab, Sci. Rep. 13 (2023) 5987.
[32] M.A.J. Kouhbanani, S. Mosleh-Shirazi, N. Beheshtkhoo, S.R. Kasaee, S. Nekouian, S. Alshehery, H. Kamyab, S. Chelliapan, M.A. Ali, A.M. Amani, J. Drug Deliv. Sci. Technol. 85 (2023) 104541.
[33] M. Sarani, M. Roostaee, M. Adeli-Sardou, D. Kalantar-Neyestanaki, S.A.A. Mousavi, A. Amanizadeh, M. Barani, A. Amirbeigi, J. Trace Elem. Med. Biol. 81 (2024) 127325.
[34] X. Gong, N.D. Jadhav, V.V. Lonikar, A.N. Kulkarni, H. Zhang, B.R. Sankapal, J. Ren, B.B. Xu, H.M. Pathan, Y. Ma, Z. Lin, E. Witherspoon, Z. Wang, Z. Guo, Adv. Colloid Interface Sci. 323 (2024) 103053.
[35] A. Menichetti, A. Mavridi-Printezi, D. Mordini, M. Montalti, J. Funct. Biomater. 14 (2023) 244.
[36] M.R. Kabir, M.M. Hasan, M.R. Islam, A.R. Haque, S.K. Hasan, J. Food Process. Preserv. 45 (2021) e15191.
[37] T. Dang-Bao, T.S. Nguyen, N.T. Tran-Dinh, H.H. Lam, H.P. Phan, Chemical Physics Impact 6 (2023) 100245.
[38] R. Thach-Nguyen, H.H. Lam, H.P. Phan, T. Dang-Bao, RSC Adv. 12 (2022) 35436–35444.
[39] H. Guo, F. Han, H. Shang, S. Xiong, M. Huynh, L. Thistle, L. Meng, L. He, B. Xing, Environ. Sci.: Nano 8 (2021) 1580–1592.
[40] M. Ismail, S. Gul, M.I. Khan, M.A. Khan, A.M. Asiri, S.B. Khan, Green Processing and Synthesis, vol. 8, 2019, pp. 118–127.
[41] D. Khwannimit, R. Maungchang, P. Rattanakit, Int. J. Environ. Anal. Chem. 102 (2022) 5247–5263.
[42] T. Bruna, F. Maldonado-Bravo, P. Jara, N. Caro, Int. J. Mol. Sci. 22 (2021) 7202.
[43] C.G.A. Das, V.G. Kumar, T.S. Dhas, V. Karthick, K. Govindaraju, J.M. Joselin, J. Baalamurugan, Biocatal. Agric. Biotechnol. 27 (2020) 101593.
[44] S. Tang, J. Zheng, Adv. Healthcare Mater. 7 (2018) 1701503.
[45] I.X. Yin, J. Zhang, I.S. Zhao, M.L. Mei, Q. Li, C.H. Chu, Int. J. Nanomed. 15 (2020) 2555–2562.
[46] G. Li, L. Liu, Y. Sun, H. Liu, J. Cluster Sci. 29 (2018) 1193–1199.
[47] J. Kim, B. Pitts, P.S. Stewart, A. Camper, J. Yoon, Antimicrob. Agents Chemother. 52 (2008) 1446–1453.
[48] E. Menumerov, R.A. Hughes, S. Neretina, Nano Lett. 16 (2016) 7791–7797.
[49] R.D. Neal, Y. Inoue, R.A. Hughes, S. Neretina, J. Phys. Chem. C 123 (2019) 12894–12901.
[50] R. Thach-Nguyen, T. Dang-Bao, IOP Conf. Ser. Mater. Sci. Eng. 1258 (2022) 012014.
[51] T. Dang-Bao, L.N. Nguyen, H.H. Lam, Mater. Today: Proc. (2023), https://doi.org/10.1016/j.matpr.2023.01.386.
[52] Y.R. Mejía, N.K.R. Bogireddy, RSC Adv. 12 (2022) 18661–18675.
[53] M.T. Ly, T. Dang-Bao, M.T.K. Nguyen, H.H. Lam, T.K.A. Tran, H.P. Phan, J. Mol. Struct. 1309 (2024) 138274.
[54] F. Lin, R. Doong, Appl. Catal. Gen. 486 (2014) 32–41.
[55] A.I. Ayad, D. Luart, A.O. Dris, E. Guénin, Nanomaterials 10 (2020) 1169.
[56] S.R. Thawarkar, B. Thombare, B.S. Munde, N.D. Khupse, RSC Adv. 8 (2018) 38384–38390.
[57] M.A. Mahmoud, F. Saira, M.A. El-Sayed, Nano Lett. 10 (2010) 3764–3769.
[58] Y.C. Chang, D.H. Chen, J. Hazard Mater. 165 (2009) 664–669.
[59] C. Dey, D. De, M. Nandi, M.M. Goswami, Mater. Chem. Phys. 242 (2020) 122237.
[60] A.D. Verma, R.K. Mandal, I. Sinha, Catal. Lett. 145 (2015) 1885–1892.
[61] J. Singh, A. Mehta, M. Rawat, S. Basu, J. Environ. Chem. Eng. 6 (2018) 1468–1474.
[62] K.F. Princy, A. Gopinath, Polar Science 30 (2021) 100692.
[63] N. Chouhan, R. Ameta, R.K. Meena, J. Mol. Liq. 230 (2017) 74–84.
[64] A. Gangula, R. Podila, M. Ramakrishna, L. Karanam, C. Janardhana, A.M. Rao, Langmuir 27 (2011) 15268–15274.
[65] Z. Shah, S. Hassan, K. Shaheen, S.A. Khan, T. Gul, Y. Anwar, M.A. Al-shaeri, M. Khan, R. Khan, M.A. Haleem, H. Suo, Mater. Sci. Eng. C 111 (2020) 110829.
[66] K. Philippot, P. Serp, Concepts in nanocatalysis, in: P. Serp, K. Philippot (Eds.), Nanomaterials in Catalysis, Wiley-VCH GmbH, Weinheim, Germany, 2013, pp. 1–54.